The tempo of greening in the European Alps: Spatial variations on a common theme

Philippe Choler, Arthur Bayle, Bradley Carlson, Christophe Randin, Gianluca Filippa, Edoardo Cremonese

Title

1 The tempo of greening in the European Alps: spatial variations on a common theme

2 **Running Title:**

3 The tempo of greening in the European Alps

4

List of authors & institutional affiliations

5 Philippe Choler[1,*], Arthur Bayle[1], Bradley Z. Carlson[2], Christophe Randin[3], Gianlucca
6 Filippa[4], Edoardo Cremonese[4]

7 1- Univ. Grenoble Alpes, Univ. Savoie Mont Blanc, CNRS, LECA, F-38000 Grenoble,
8 France

9 2- Centre de Recherches sur les Écosystèmes d'Altitude (CREA), Observatoire du Mont-
10 Blanc, F-74400 Chamonix, France

11 3- Univ. Lausanne, Dept. of Ecology & Evolution / Interdisciplinary Centre for Mountain
12 Research (CIRM), Biophore, CH-1015 Lausanne, Switzerland

13 4- Environmental Protection Agency of Aosta Valley, Climate Change Unit, Loc. La
14 Maladière, 48, IT-11020 Saint-Christophe (AO), Italy

15

16 **Contact Information**

17 Philippe Choler, +33 6 76 51 48 96, philippe.choler@univ-grenoble-alpes.fr

18

19

Key words

mountain ecosystems - climate change - European Alps - greening - NDVI - remote sensing

Abstract

The long-term increase of satellite-based proxies of vegetation cover is a well-documented response of seasonally snow-covered ecosystems to climate warming. However, observed greening trends are far from being uniform and substantial uncertainty remains concerning the underlying causes of this spatial variability. Here, we processed surface reflectance of the moderate resolution imaging spectroradiometer (MODIS) to investigate trends and drivers of changes in the annual peak values of the Normalized Difference Vegetation Index (NDVI). Our study focuses on the above treeline ecosystems in the European Alps. The NDVI changes of these ecosystems are highly sensitive to land cover and biomass changes and are marginally affected by anthropogenic disturbances. We found a widespread greening for the period 2000-2020, a pattern that is consistent with the overall increase of summer temperature. At the local scale, the spatial variability of greening was mainly due to the preferential response of north-facing slopes between 1900 m and 2400 m. Using high resolution imagery, we noticed that the presence of screes and outcrops exacerbated this response. At the regional scale, we identified hotspots of greening where vegetation cover is sparser than expected given the elevation and exposure. Most of these hotspots experienced delayed snowmelt and green-up dates in recent years. We conclude that the ongoing greening in the Alps primarily reflects the high responsiveness of sparsely vegetated ecosystems that benefitted the most from temperature and water-related habitat amelioration above treeline.

Introduction

The long-term increase of greenness in cold, seasonally snow-covered ecosystems is widely perceived as a consequence of climate change (Berner et al., 2020; Keenan & Riley, 2018) . Arctic and alpine ecosystems have undergone particularly fast greening compared to other ecosystems and this is consistent with the accelerated warming documented for these regions (Callaghan et al., 2010; Pepin et al., 2015). However, this greening exhibits considerable spatial and temporal variability that is far from being understood (Berner et al., 2020; Cortés et al., 2021; Ju & Masek, 2016; Myers-Smith et al., 2020). The complex interaction between regional climate trends, topography, geomorphological and other disturbance regimes and vegetation dynamics contributes to these non-uniform patterns of greening (Ropars & Boudreau, 2012; Tape, Hallinger, Welker, & Ruess, 2012). Further studies are required to document the relative contribution of these drivers and to advance a more predictive understanding of greening and its consequences on ecosystem processes and services (Duveiller, Hooker, & Cescatti, 2018; Forzieri, Alkama, Miralles, & Cescatti, 2017; Myers-Smith et al., 2020; Zhu et al., 2016).

Temperate mountains have experienced warmer summers over the last decades (Beniston, 2006; Hock et al., 2019). Several studies have underlined the impact of these changes on land surface phenology (Asam et al., 2018; Dunn & de Beurs, 2011; Xie et al., 2020; Zhang, Zhang, Dong, & Xiao, 2013), ecosystem productivity (Choler, 2015; Jolly, Dobbertin, Zimmermann, & Reichstein, 2005), and species richness (Lamprecht, Semenchuk, Steinbauer, Winkler, & Pauli, 2018; Steinbauer et al., 2018). Other studies reported on the long-term increase of greenness in the south-western Alps (Carlson et al., 2017; Filippa et al., 2019), the Hindu Kush(Anderson et al., 2020) and underlined the particular responsiveness of sparsely vegetated areas located in the nival belt. However, none of these studies has provided a comprehensive analysis of the spatial variability of greening at the mountain range scale and

an investigation of its determinants. More specifically, the distinction between exposure to change (e.g. climate) and the responsiveness of ecosystems to change has remained elusive. Yet, well-documented case studies in the Arctic suggest that this fundamental question may underpin much of the observed spatial complexity of greening. For example, the preferential expansion of arctic shrubs in particular topographical situations - such as along streams or in floodplains, lead to local-scale greening heterogeneity (Tape, Sturm, & Racine, 2006), which in turn is possibly related to the snow-holding capacity of shrubs in winter(Sturm et al., 2005). The initial cover of *Betula glandulosa* in the 1950s explained part of the spatial variability of greening in Nunavik (Ropars & Boudreau, 2012; Ropars, Levesque, & Boudreau, 2015). These studies pointed out that land cover properties are pivotal to predict the responsiveness of the system to on-going changes and to identify the underlying ecological mechanisms of greening.

There is a growing body of evidence showing that mountain ecosystems of the Alps have undergone rapid changes in response to climate warming (Gottfried et al., 2012). Plot-based long-term surveys revealed increasing vegetation cover in mountain grasslands, mainly due to the expansion of graminoids (Rogora et al., 2018) and a colonization of screes and outcrops by shrubs and trees (Vittoz, Bodin, Ungricht, Burga, & Walther, 2008). While these studies are invaluable to inform on ecological mechanisms underpinning ecological changes, their paucity precludes tracking complex, non-linear responses along topographical, geomorphological and climate gradients. For example, winter snow duration - which is widely acknowledged as a key driver of vegetation dynamics - for the time being shows decreased sensitivity to global warming at elevations above 2000 m (Hantel & Hirtl-Wielke, 2007; Schoener, Koch, Matulla, Marty, & Tilg, 2019). Another issue is the overrepresentation of high summits in plot-based surveys, considering that the area they cover represents a minute fraction of the land above treeline. For these reasons, remote sensing offers a complementary

89 approach to probe ongoing land cover changes at a scale encompassing multiple
90 environmental gradients and to examine their impacts on ecosystem services such as water
91 provisioning, carbon sequestration or pastoral resources.
92 Here, we exploit available time series of the moderate resolution imaging
93 spectroradiometer (MODIS) to provide a comprehensive picture of recent greening and its
94 spatial variability in the European Alps and to improve our understanding of its drivers. Our
95 study utilizes annual peak values of the Normalized Difference Vegetation Index (NDVI) as a
96 proxy of land surface greenness (Tucker, 1979). We quantified the significance and
97 magnitude of NDVI trends for high elevation ecosystems that are located between the treeline
98 and the permanent snowline. This allows us to overcome two potential issues in such remote
99 sensing studies. First, high elevation ecosystems are less affected by anthropogenic
100 disturbances than other European habitats at lower elevation, which should facilitate the
101 unraveling of a climate signal on greening trends (Filippa et al., 2019; Gehrig-Fasel, Guisan,
102 & Zimmermann, 2007). Second, the NDVI range of these ecosystems lies in a range where it
103 is highly sensitive to land cover and biomass changes, in contrast to closed canopies where
104 NDVI no longer linearly depends on biomass or plant cover (Huete et al., 2002; Myneni &
105 Williams, 1994).
106 We addressed the three following questions:
107 1. How widespread is the greening signal in above-treeline ecosystems of the
108 European Alps?
109 2. Is the variability of greening spatially structured and what are its main drivers?
110 3. Are there fine scale land cover features that predispose to fast greening response?

Material and methods

Study area and selection of pixels

The European Alps is a mountain range stretching over 1'200 km from Nice (France) to Vienna (Austria). Our study focuses on the uplands of the massif that are located between the treeline and the permanent snowline. This area includes shrublands, grasslands and sparsely vegetated ecosystems established on screes, debris, and outcrops. We first selected a set of 250-m resolution MODIS pixels having non-forested land cover classes with a tree cover density below 5%, an elevation above 1400 m and an average NDVImax above 0.15. To do so, we relied on a 25-m resolution Digital Elevation Model, a 100-m resolution Tree Cover Density of year 2018 (https://land.copernicus.eu/pan-european/high-resolution-layers/forests/tree-cover-density/) and the Corine Land Cover (CLC) product of year 2018 (https://land.copernicus.eu/pan-european/corine-land-cover/), which is based on the visual photointerpretation of aerial images at a 100-m resolution. From the 44 CLC entries at level 3, we retained the following classes: Pastures (code 2.3.1), Natural grasslands (code 3.2.1), Moors and heathlands (code 3.2.2), Bare Rocks (code 3.3.2), Sparsely vegetated (code 3.3.3). We merged pastures and grasslands and we renamed the misleading "bare rocks" to "very sparsely vegetated" as we selected pixels with an average NDVImax above 0.15, i.e. not completely devoid of vegetation. We discarded pixels exhibiting more than 10% of settlements (ski resorts) or permanent water using data layers of European settlements (https://land.copernicus.eu/pan-european/GHSL/european-settlement-map/) and of permanent water (https://land.copernicus.eu/pan-european/high-resolution-layers/water-wetness/status-maps/water-wetness-2018). We also removed pixels for which we found significant abrupt changes of NDVImax within the period 2000-2020, as this might be indicative of a physical or anthropogenic disturbance unrelated to climate trend. This was done by using the Breaks For Additive Seasonal and Trend (BFAST) on 8-days NDVI time series. Breaks were identified after the time series decomposition into trend, seasonal and remainder component.

Abrupt changes were considered as break points when their uncertainty was found to be smaller than one year, consistent to a previous study in the south-western Alps (Filippa et al., 2019). This led to discard around 5 % of the total number of pixels. We ended up with 511,375 pixels of which 284,346 (55.6%) exhibited an average NDVImax below 0.65. Our main findings are based on this data subset to avoid the annoying saturation effect of NDVImax for closed canopies (see Introduction and Figure S2). Figure S3 and Table S1 give the spatial distribution of these pixels and their breakdown by administrative units using the Nomenclature of territorial units for statistics (NUTS) classification at level 3 (https://ec.europa.eu/eurostat/web/gisco/geodata/reference-data/administrative-units-statistical-units/). Figure S12 shows the distribution of pixels per elevation and DAH classes. We processed all spatial data using the raster, rgdal, sp and proj4 R packages (Venables & Ripley, 2002). We used the bfast R package to implement the BFAST analysis (Verbesselt, Hyndman, Newnham, & Culvenor, 2010).

Estimates of MODIS-derived NDVI metrics

We downloaded the 250-m resolution 8-day composite of MOD09Q1/Terra collection 6 products that are available in hdf format at the Land Processes Distributed Active Archive Center (https://e4ftl01.cr.usgs.gov/). Acquired dates covered the period from 18 February 2000 to 27 December 2020. We assembled the tiles h18.v4 and h19v04, to cover the entire massif and re-projected red and near-infrared (NIR) surface reflectance values (ρ) in the EPSG 3035 geometry. We retained reflectance values produced with high quality (according to the MOD09Q1 Quality Control flag) and calculated a NDVI according to $(\rho_{NIR} - \rho_{RED})/(\rho_{NIR} + \rho_{RED})$, where ρ is reflectance. We did not to use the 500m-resolution 16-day composite BRDF-corrected MODIS products (MCD43A4) as we needed a higher temporal and spatial resolution to best capture the peakiness of NDVI changes during the short growing season

above treeline. Raw NDVI time series were processed in two steps. First, we used the Best Index Slope Extraction (BISE) algorithm to reduce the noise of the NDVI time series (Viovy, Arino, & Belward, 1992) with the parameters: n=0.2 (i.e. a 20% acceptable difference in NDVI values within the sliding period) and p=3 (the length of the forward sliding period). Second, we applied a low-pass filter using the Savitzky-Golay algorithm (Savitzky & Golay, 1964) with the following parameters: n=3 (the filter order) and p=7 (the filter length). Smaller values of p would allow keeping track of more rapid changes whereas higher values would increase the smoothing. We also estimated a green-up date as the first date of the year where the NDVI amounts 50% of the NDVImax. This was achieved using daily-interpolated time series of NDVI. This date is highly correlated to snow melting in the high-elevation mountain grasslands of the Alps (Choler, 2015; Fontana, Rixen, Jonas, Aberegg, & Wunderle, 2008). We used the non-parametric, rank based, Mann–Kendall (MK) monotonic test to assess the significance of NDVI time series trends. The significance was given by the approximately normally distributed z score with z values > 1.96 indicating a significant increase (*P-value* <0.05) and z values < -1.96 a significant decrease (at *P*-value <0.05). To quantify change over the period 2000-2020 we fitted linear models based on Theil-Sen single median slope. The Theil-Sen estimator of the linear trend is much less sensitive to outliers than the least-squares estimator. The distribution of NDVImax slopes for the different ranges of NDVImax values is shown in figure S2. The decrease of the slopes in the highest ranges of NDVImax was clearly indicative of a saturation effect. For further analyses, we retained pixels with a NDVImax value between 0.15 and 0.65. In this range, the pairwise mean difference of greenness slopes was below 0.005 (Figure S2). We randomly perturbed the RED and NIR raw reflectances by up to +/- 5% to and recalculated 1000 times the MK trends and the Theil-Sen slopes for all pixels. The uncertainty of MODIS reflectance, and therefore of vegetation indices, arises from sensor calibration and the different steps of atmospheric correction (Vermote & Vermeulen,

1999). A perturbation of 5% lies in the upper range of the uncertainties associated with MODIS products(Miura, Huete, & Yoshioka, 2000). Our numerical simulation propagates this uncertainty into the estimates of NDVI trends and ensures a more robust analysis of the drivers of greening using random forest. We used the Kendall R package for estimating Mann-Kendall trends (McLeod, 2005) and the signal R package for the Savitzky-Golay function (signal developpers, 2013).

Preparation of predictor datasets

We estimated terrain indices from the 25 m resolution European Digital Elevation Model (EU-DEM, version 1.0, https://land.copernicus.eu/imagery-in-situ/eu-dem/). We resampled the EU DEM at a 250 m resolution and calculated the mean, range and standard deviation of elevation and the Diurnal Anisotropic Heating (DAH). The DAH index approximates the anisotropic heating of land surface to radiation (Böhner & Antonić, 2009). We computed DAH as $\cos(\alpha_{max} - \alpha) \cdot \arctan(\beta)$ where α is the aspect, β is the slope and the parameter α_{max} corresponds to the aspect with the maximum total heat surplus. We used α_{max} = 212° as we noticed that this SSW orientation corresponds on average to the earliest First Snow Free Day derived from Sentinel-2 products in the south-western Alps (unpublished results). Bedrock data were extracted from the 1:1 million OneGeology pan-European harmonized surface geological maps distributed by the European Geological Data Infrastructure (EGDI) portal (http://www.europe-geology.eu/). Surface geological units were aggregated into four categories: (i) igneous and metamorphic rocks including granite, gneiss etc., (ii) ferromagnesian rocks including serpentines, amphibolite, andesite, basalt etc., (iii) hard sedimentary rocks including dolomite, limestone etc. and (iv) clastic rocks including schist, mudstone, shale, flysch etc. For climate trends, we used the daily-based gridded datasets of E-OBS at a 0.1° resolution for the period 1995 onwards (version E-OBS v22.0e,

https://surfobs.climate.copernicus.eu/dataaccess/access_eobs.php) (Cornes, van der Schrier, van den Besselaar, & Jones, 2018). For each year, we calculated Growing Degree Days (GDD) as the cumulative sum of daily average air temperature above 0°C during the summer months (June, July and August). As a complementary estimate of summer warming, we also extracted the average of daily maximum temperatures in July (T07). We computed a climatic water balance as the difference between precipitation (P) and a reference crop evapotranspiration ET_0. We summed the P-ET_0 difference over the summer months to assess the dry–wet conditions of the growing season. ET_0 was estimated on a daily basis using the equation $\lambda ET_0 = C\ (\Delta/\Delta+\gamma)\ Q$, where Q is the global radiation (MJ m^{-2} day^{-1}), Δ the slope of the vapour pressure-temperature curve (kPa $°C^{-1}$), γ the psychometric constant (kPa $°C^{-1}$), λ the latent heat of vaporization (MJ kg^{-1}), and C an empirical coefficient (C=0.65). This is a simplified version of the Penman–Monteith equation originally proposed by Makkink and later modified by Hansen (Hansen, 1984). Maps of climate predictors are shown in figures S9 and S10. For snow cover duration trends in the French Alps (Figure S11), we used the S2M meteorological and snow cover re-analysis for the period 1959-2019 (https://www.aeris-data.fr/catalogue/) (Vernay et al., 2019). As for NDVI time series, we used the non-parametric Mann–Kendall (MK) monotonic test and the Theil-Sen median slope to assess the significance and the magnitude of decadal trends of all meteorological variables.

Random forest analysis.

We implemented a random forest analysis to identify the best predictors of the spatial variability of greening. Based on the Mann-Kendall significance tests, we classified the greenness trends into three categories: no significant greening (P-value > 0.05), moderate greening (0.001<P-value<0.05) and strong greening (P-value <0.001). There were not enough pixels exhibiting browning to include this response in the analysis. We randomly sampled

15 000 pixels in each category to balance the sample size among the greening responses and partitioned the data set into a model training subset (two thirds of pixels) and a model evaluation subset (one third of pixels). We repeated this procedure 1000 times, meaning that we assembled one random dataset for each perturbed simulation of MODIS reflectance and implemented one Random Forest model for each dataset. Predictor variables included elevation, Diurnal Anisotropic Heating, bedrock, NDVImax anomaly and decadal trends for the green-up date and the climate variables GDD and $P\text{-}ET_0$. We calculated pair-wise correlations between predictors and checked that they were not highly correlated, i.e. $r < 0.5$ (Figure S13). We also implemented a Random Forest model including NDVImax to check for its influence on the classification probability and to further document the saturation effect (Figure S6). We relied on the out-of-bag classification accuracy to select the best Random Forest model. We assessed predictor importance using the mean decrease in accuracy metric, which is indicative of suitability of predictor, and the mean decrease in Gini, which is indicative of the homogeneity of nodes and leaves. Predictor importance was based on a permutation-based importance measure where one measures the effect of reshuffling each predictor on model accuracy. Last, we examined how classification probabilities depend on the values taken by each predictor by computing partial dependence plots. We computed empirical cumulative distribution function to determine the range of values where interpretation of partial dependence plots needs caution due to small sample size. We used the randomForest, caret, and pdp R packages to implement Random Forest models and evaluate its performance (Greenwell, 2017; Kuhn, 2020; Liaw & Wiener, 2002).

Land cover assessment using very high-resolution imagery.

Using the high-resolution imagery of Google Earth, we characterized the land cover features of a selection of 300 500m x 500m cells. First, we aggregated NDVImax anomaly at

a 500 m resolution. Then we performed a stratified random sampling of pixels using three classes of NDVImax anomaly - negative, around zero and positive values - and 100 pixels in each class (Figure S7). The visual photointerpretation of very high-resolution imagery from Google Earth allows us to distinguish 6 types of object: singular trees or tree patches, tall shrubs or shrublands (mainly composed of *Pinus mugho*), low shrublands (presumably *Ericaceae*-dominated), grasslands, screes and debris and finally outcrops. We assigned a percentage cover to these classes using the semi-quantitative ranges: <5%, 5%-25%, 25%-50%, 50%75% and 75%-100%. Three authors of this paper (PC, EC, GF) conducted the photointerpretation independently and we retained the most frequent cover estimate for each land cover class. We did not try to standardize the year of satellite view, as there were no sufficient good quality images to do it.

Results

Over the 2000-2020 period, we found significant (P<0.05) positive temporal trends of NDVImax for 56% of the 284,346 analyzed pixels and significant negative trends for less than 0.1% of all pixels (Figure 1a and Table S1). Irrespective of significance, the ratio between positive and negative slopes was 26/1. These results were robust to uncertainty in MODIS data as more than two thirds of the pixels classified as fast (P<0.005) and non-significant greening (P>0.05) remained in these two classes when reflectance values were randomly perturbed (Figure S1). Sparse and very sparse vegetation contributed to 23% and 26% respectively of the 56% of significant greening compared to 7% for grasslands and heathlands (Figure 1b). Figure S2 shows that there was no strong effect of the average NDVImax on the magnitude of greening in the selected range (0.15-0.65). By contrast, there was a marked decline in greening for higher values of NDVImax suggesting a saturation

285 effect (Figure S2 and Table S1). Only 31% of pixels exhibited a significant greening when the
286 NDVImax value was above 0.65, the (Table S1).

287 Although widely distributed, the greening trends are not spatially uniform (Figure 2).
288 We found a regional-scale component of this spatial variability, with hotspots of greening
289 corresponding to southern parts of the French Alps (e.g. Haute-Provence and Maritime Alps,
290 France), the southern part of the Central Alps (e.g. Sondrio, Italy and Tiroler Oberland,
291 Austria) and the Northeastern-most part of the Alps (e.g. Pinzgau-Pongau, Austria; Figure 2,
292 S3 and Table S1). At the local scale, topographical factors also modulate the greening trends
293 (Figure 3a). First, there is a general tendency for the greening to increase with elevation
294 (Figure 3a). Second, and on top of that, the greening is more noticeable for north-facing steep
295 slopes i.e. for the most negative values of diurnal anisotropic heating (DAH), a proxy of the
296 heating of land surface to radiation (Figure 3a). Consequently, we observed an overall upward
297 shift of the isolines of NDVImax, meaning that the elevation of given value of NDVImax has
298 increased steadily over the last two decades (Figure 3b). We estimated the median of this shift
299 at 45 m per decade with strong regional disparities (Figure S4). It is worth noting that the
300 magnitude of this elevational shift is higher for the first deciles of the distribution than for the
301 last, and this difference is particularly striking at negative DAH values (Figure 3b). These
302 results point out that greening is enhanced when the NDVImax is below the median of the
303 distribution for a given elevation and DAH, leading to a reduction of the interdecile
304 differences in the distribution of NDVImax along topographical gradients (Figure 3b).

305 These findings prompted us to quantify a per-pixel NDVImax anomaly and to assess
306 its spatial distribution in the European Alps. The anomaly was calculated as the difference
307 between the average NDVImax of a given pixel and the median NDVImax value of all pixels
308 lying in the same class of DAH and elevation (Figure 4a). Negative anomalies are indicative
309 of an “abnormally” low NDVImax value with respect to elevation and DAH. The mapping of

this anomaly revealed a clear regional-scale variability that was partly congruent with that of greening (Figure 4b). For example, the southern part of the French Alps, part of the south Central Alps and the Northeastern-most Alps are regions that present a combination of fast greening (Figure 2), negative NDVImax anomalies (Figure 4b), and high upward shift of NDVImax (Figure S4).

We evaluated the importance of this NDVImax anomaly in predicting the observed greening trends against two sets of predictors that are more widely used in greening studies, i.e. topographical predictors (elevation and DAH) and climate predictors pertaining to the growing season (summer). We used trends in the accumulation of growing degree-days (GDD) during summer as a proxy of temperature-related changes and trends in the difference between precipitation and potential evapotranspiration as a proxy of water balance-related changes (see Methods). We also estimated trends in the green-up date derived from the analysis of NDVI time series. Previous studies showed that the green-up date strongly depends on snow cover duration in high elevation temperate ecosystems (Choler, 2015). We built a random forest model to assess the usefulness of these variables for classifying pixels into three categories based on the Mann-Kendall significance test - no greening ($P>0.05$), moderate greening ($P<0.05$) and fast greening ($P<0.005$). The model classified the "no greening" and the "fast greening" classes with an accuracy of 61.5% and 62 % respectively corresponding to a kappa of 0.42 and 0.4 (Table S3). The values of the first and ninth deciles of the 1000 simulations differ by less than 2% from the mean. The performance of the random forest classifier for the "moderate greening" was low with an overall accuracy of 0.51 to be compared to a random accuracy of 0.33 (Table S3). The ranking of predictors shows that the NDVImax anomaly is as important as climate predictors (Figure 5a,b). Noticeably, its score is high for both the mean decrease accuracy and the mean decrease in Gini coefficient, indicating a high suitability as a predictor and a high contribution to the homogeneity of

nodes and leaves. By contrast, climate predictors show high decrease in permutation tests but do not exhibit a high contribution to the purity of nodes (low mean decrease in Gini), while topographical predictors show the reverse trend (Figure 5b). The greening trends did not change between bedrock types (Figure S5) and bedrock exhibited a very low variable importance in random forest. For these reasons, it was not retained in further analysis. Partial dependence plots (Figure 5c) reveal that greening was mostly associated with negative NDVImax anomalies, negative DAH, elevation between 2300 m and 2700 m and increasing green-up dates, and was marginally enhanced by a more positive trend in GDD and water balance. The lack of greening occurs more often at low and very high elevation, where NDVImax anomaly was positive and green-up dates decrease and, to a lesser extent, where climate amelioration was weak (Figure 5c). Given the positive correlation between snow melting date and green-up date above treeline, our results indirectly pointed out to a positive effect of delayed snow melt on the recent greening trends. We also implemented complementary random forest models for subsets of pixels lying in narrower ranges of NDVImax (0.15-0.4 and 0.4-0.65) and by adding NDVImax as a supplementary predictor (Figure S6). The ranking of variable importance was consistent for all these simulations, which also confirmed the overwhelming importance of the NDVImax anomaly for predicting the greening response whatever the NDVImax value (Figure S6). They also pointed out that adding the NDVImax as a supplementary predictor tends to lower the importance of the NDVImax anomaly (Figure 5a and S6a), which is explainable by the positive correlation between these two variables.

The strong link between negative NDVImax anomalies and significant greening trends led us to explore at a finer scale the land cover features associated with these contexts. Using very high-resolution satellite imagery from Google Earth, we performed a visual photo-interpretation of 300 randomly selected sites across the Alps (Figure S7). First, this analysis

360 indicated that NDVImax anomalies were consistently negative in the case of high cover of
361 screes, debris and outcrops (Figure 6a). The reverse trend holds for grassland cover (Figure
362 6c). Second, the magnitude of greening tend to increase with the cover of screes and debris
363 and decreases with that of grasslands (Figure 6b,d). Last, we did not find evidence that the
364 presence of nearby trees or tall shrubs was associated with more frequent greening, suggesting
365 that the densification of non-woody vegetation is as important as the upward shit of trees to
366 explain greening. This is illustrated by four examples of land cover dynamics using past and
367 current very high-resolution color-infrared aerial photographs that are available for the French
368 Alps (Figure S8).
369

Discussion

370 The main findings of our study are threefold. First, more than half of the land surface
371 occupied by above-treeline ecosystems in the European Alps has experienced significant
372 greening over the last two decades. By contrast, the number of pixels showing significant
373 browning trends is less than 1%. Second, this widespread greening is spatially non-uniform,
374 and fast greening responses can be explained by a combination of local-scale factors - i.e.
375 elevation and exposure - and regional-scale factors pertaining to anomalies of NDVImax and
376 trends in green-up dates. Third, we provided substantial evidence for the high responsiveness
377 of north-facing and sparsely vegetated areas that have clearly benefited the most from recent
378 climate changes in the European Alps.
379 Our study investigated greening trends across a vast and highly heterogeneous
380 landscape. Above-treeline ecosystems in the Alps include a wide range of geomorphological,

topographical and ecological situations that lead to a high turnover of plant communities over short distances. This fine-scale heterogeneity in plant cover inevitably calls into question the appropriateness of using moderate resolution remote sensing products to assess greening trends in mountainous landscapes. For example, it is entirely possible that contrasting trends of greenness are occurring within a 250 m resolution pixel because of habitat-specific responses (Matteodo, Ammann, Verrecchia, & Vittoz, 2016). While the use of moderate resolution remote sensing products certainly limits our ability to assign specific NDVImax trajectories to particular plant communities or habitats, our approach nonetheless provides a very valuable and comprehensive picture of vegetation shifts at the mountain range scale, and enables broad-scale investigation of land cover dynamics as demonstrated in previous studies (Zhao & Running, 2010). We acknowledge the potential of using high-resolution products such as the Landsat archive to complement our study. However, this will raise other difficulties. The most critical is the low frequency of available images, which makes it difficult to capture the peak of growth in alpine environments, and leads to large uncertainties in the estimate of NDVImax. In addition, calculating a finer grained greening response would exacerbate the mismatch between the spatial scale of remote sensing products and that of drivers of changes, especially climate (Randin et al., 2020). For these reasons, we believe that high-resolution remote sensing data would be more appropriate to examine the response of specific habitats or sites for which ground-truthing data are available. Similarly, the utilization of aerial photograph archives has an enormous, yet largely unexplored, potential to relate very fine-grained land cover dynamics to observed greening trends (see illustrative examples in Figure S8)

Another difficulty of our comparative analysis of greening trends pertains to the wide range of vegetation cover that is included. It is well known that NDVI exhibits a nonlinear response to aboveground biomass and plant cover, especially for planophilous canopies

406 (Myneni & Williams, 1994). The sensitivity of NDVI to an incremental change in biomass or
407 cover decreases for dense canopies, as does our capacity to detect a significant greenness
408 trend in these contexts. Thus, one may run the risk that the spatial variability of greening
409 partly reflects the different sensitivity of the method used to detect greening. We paid
410 particular attention to this issue and removed from our analysis all pixels with high NDVImax
411 values (> 0.65), as we had clear indications of a saturation effect on greening (Figure S2). The
412 relationship between NDVImax and biomass or cover is linear in the NDVImax range we
413 selected (Myneni & Williams, 1994). We also performed similar random forest analyses on
414 subsets of pixels exhibiting very low NDVImax value and found similar conclusions (Figure
415 S6). For these reasons, we are confident that the saturation of NDVImax with aboveground
416 biomass did not blur our assessment of greening trends in the European Alps.
417 Our report on widespread greening in above-treeline ecosystems of the Alps is
418 consistent with previous studies on arctic and alpine ecosystems (Berner et al., 2020; Ju &
419 Masek, 2016; Krakauer, Lakhankar, & Anadon, 2017; Xie et al., 2020). As in other cold parts
420 of the earth, high elevation ecosystems of the Alps have experienced a more pronounced
421 warming than lowlands (Palazzi, Mortarini, Terzago, & von Hardenberg, 2019; Pepin et al.,
422 2015) and, not surprisingly, these temperature-limited ecosystems are benefitting from this
423 increased temperature. However, and by comparison to a recent report from the Arctic
424 (Berner et al., 2020), we found very few significant browning trends. A plausible explanation
425 is that all regions of the Alps have experienced warmer summers, albeit to varying degrees,
426 over the last decades (Figure S9). This led us to consider that, at least for the Alps, the
427 knowledge gap is less about the detection of significant greening trends than it is about the
428 causes of its spatial variability in a warmer climate. Our study provides new perspectives on
429 this matter, given that we unraveled the pivotal role of the anomaly of NDVImax to capture
430 part of this greening complexity. Ecosystems exhibiting a lower NDVImax than expected

given the topography, i.e. a negative anomaly, have been the most responsive over the last two decades, and this is the reason why we observe today a reduced dispersion of NDVImax values for a given elevation x DAH compared to the years 2000 (Figure 4b) as well as reduced regional heterogeneity (Figure 2). We can refer to this trend as a *catching-up phenomenon* and we assert that it is the most important facet of the ongoing greening in the Alps.

To further understand this phenomenon, we paid particular attention to land cover properties using high-resolution images. Clearly, the presence of very sparsely vegetated surfaces - such as screes, talus and outcrops - is a predisposing factor to negative anomalies and greening (Figure 6). In this regard, our findings extend at a broader mountain range scale conclusions that were drawn from more localized studies (Carlson et al., 2017). The increasing vegetation cover in initially sparsely vegetated areas is being documented through long-term surveys (Rixen, Wipf, Frei, & Stoeckli, 2014; Steinbauer et al., 2018) and remote sensing (Carlson et al., 2017). Noticeably, several reports have underlined the preferential expansion of tall shrubs and trees on screes and debris compared to nearby grasslands. In addition to forest ingrowth caused by land-use abandonment, this upward shift of trees is the other dimension of tree expansion documented in the Alps (Gehrig-Fasel et al., 2007; Vittoz, Rulence, Largey, & Frelechoux, 2008), and diffuse treelines can be highly responsive to climate warming (Harsch, Hulme, McGlone, & Duncan, 2009). Forest dynamics at the treeline have also been influenced by the constant decline of pastoralism and the related human activities due to the land abandonment since the Industrial Revolution (1850), making it difficult to disentangle climate influence and human impacts (Motta & Nola, 2001). In the southern part of the Alps, these dynamics occur well above the treeline, which is mainly constituted by the European larch (*Larix decidua* L.) and the stone pine (*Pinus cembra* L.). For example, the systematic survey of alpine ridges and cliffs in the south-western Alps led to

report on the occurrence of isolated individuals or stands of *Pinus cembra* at very high elevation (André, Lavergne, & Carcaillet, 2020). This is consistent with the hypothesis that the upward shift of the treeline may be more pronounced in the inner part of the Alps where trees take advantage of the more continental, warmer and drier, climate(Körner, 1999). Our study did not allow to precisely relate tree cover dynamics with greening because of the coarse resolution and the focus on high elevation sites. Nonetheless, we noticed that the greening trends are more accentuated on north-facing slopes that are generally more forested and more densely covered by heathlands than southern aspects. Further studies should associate the different magnitudes of increase in NDVImax to well-documented colonization of pioneer shrubs and trees. Our mapping of hotspots and coldspots of greening can provide the foundations for such an investigation coupling remote sensing and plant population models.

Another ecological dynamic that is consistent with our findings is the increasing cover of dwarf shrub - mainly *Ericaceous* species - in north-facing grasslands. Expanding low shrub cover in recent decades has been reported in the central Italian Alps at elevations up to 2500 m (Cannone, Sgorbati, & Guglielmin, 2007). Coupled with climate change, the transition from an agro-pastoral socio-economic model to an economy based on tourism and skiing has enabled a pronounced expansion of trees and shrubs into mountain grasslands in numerous locations throughout the Alps since the 1950s, including for example the Chamonix valley (unpublished data). In addition to the expansion of woody vegetation, increasing grass cover in sparsely vegetated areas is probably contributing to the observed trends, both in the context of screes and talus as well as glacier forelands in the wake of glacier retreat (Mainetti et al., 2021).

Our study allowed for distinction between external drivers of greening such as climate and predisposing factors that pertain to the initial state of the responding system. Overall, the

481 regional-scale variability of the greenness response did not strongly reflect spatial variation in
482 climate change. Several reasons may explain this phenomenon. First, the climate data we used
483 may be poor predictors because they fall short to capture surface conditions in high elevation
484 complex terrain. There are a limited number of weather stations above 2000 m in the Alps,
485 and some variables like precipitation are notoriously difficult to model along topographical
486 gradients (Frei & Isotta, 2019; Vionnet et al., 2019). Second, plant growth and community
487 dynamics primarily respond to fine-scale thermal and moisture regimes that depend on
488 landforms and soil factors (Giaccone et al., 2019; Liberati, Messerli, Matteodo, & Vittoz,
489 2019; Matteodo et al., 2016; Suding, Farrer, King, Kueppers, & Spasojevic, 2015), and these
490 factors are not accounted for in continental-scale gridded datasets. Third, high-elevation
491 ecosystems may respond to different temporal scales of climate such as extreme events or past
492 climate shifts. For example, previous studies have underlined the positive response of alpine
493 primary productivity to heat waves (Corona-Lozada, Morin, & Choler, 2019; Jolly et al.,
494 2005). There is also strong evidence that the most significant rise of temperature in the Alps
495 occurred in the late eighties (EEA, 2009), i.e. a decade before the start of the MODIS
496 observations. It is possible that these particularly favorable years lead to massive plant
497 recruitment and that we are tracking the consequences of these events years later.
498 An example of a physical variable that we can track at the pixel scale is the green-up
499 date, which strongly depends upon the first snow free date. At first glance, our findings are
500 counter-intuitive as the likelihood of greening is predominantly associated with a delayed
501 green-up date (Figure 4), as illustrated by the situation in the south-western Alps and the
502 south-central Alps (Figure S10). Using the regional climate re-analysis available for the
503 French Alps, we confirmed that the positive trend of the green-up date is consistent with
504 delayed snow melt-out during the last 20 years especially in the southern-most ranges and
505 above 2000 m (Figure S11). A significant decrease in snow-melt-out dates in the 1980s and

1990s has been reported, mostly for sites below 2000 m (Durand et al., 2009; Klein, Vitasse, Rixen, Marty, & Rebetez, 2016; Matiu et al., 2021). Recent reports highlighted that these trends tend to vanish in the recent period, especially at high elevation (Matiu et al., 2021; Vorkauf, Marty, Kahmen, & Hiltbrunner, 2021). In line with these findings, there is evidence that high elevation sites in European Alps have experienced an increase in the precipitation over the last decades (Avanzi et al., 2020; Napoli, Crespi, Ragone, Maugeri, & Pasquero, 2019). We hypothesize that the combination of snowy winters and warm summers may be particularly favorable for alpine vegetation, especially where vacant niches are available for recruitment. This was suggested by Corona et al. (2019) who showed that among the four main heat waves that hit the Alps in the last 20 years, the only one that did not translate into increased productivity was that of 2015 because a strong water deficit coincided with increased temperature. Recent work also indicated that earlier snowmelt can be detrimental to the growth of *Rhododendron ferrugineum* shrubs that preferentially occur on north-facing slopes (Francon et al., 2020). It is therefore plausible that a delayed snowmelt ameliorates the summer soil water balance and acts synergistically with warm summer temperatures to boost plant productivity and colonization, especially on north-facing slopes that may previously have been too cold to support dense vegetation cover. Further studies are needed to confirm that this association between prolonged snow cover and greening is not simply coincidental but is reflecting ecological mechanisms that are beneficial to plant recruitment and growth.

Finally, our findings call into question whether changes in pastoral management may have contributed to the negative NDVImax anomalies and more generally to the contrasting regional greening trends. Unfortunately, consistent long-term data on mountain livestock systems are not available at the scale of the European Alps. A socio-economic analysis led Tappeiner & al. (2008) to identify regions of the European Alps where agriculture receded in recent years. Most of the Italian Alps and the North-easternmost Austrian Alps were

described as “forgotten rural areas” experiencing sharp decline in agriculture, which demonstrates substantial spatial consistencies with our delineation of greening hotspots. However, the analysis aggregated many different socio-economic variables at the scale of administrative districts, and it was not possible to include it in our analysis of the drivers of greening. There is certainly no simple relation between greening trends and changes in agricultural practices. For example, there has been a remarkable resilience of mountain livestock farming systems in the southern part of the French Alps which is a greening hotspot, and this was observed despite many adverse factors such as demography, poor profitability, extreme events and return of the large predators (Hinojosa, Napoleone, Moulery, & Lambin, 2016). Recent trends even point toward an increasing demand for high-elevation pastures to overcome the detrimental effects of droughts in lowlands and southernmost mountain ranges, leading shepherds to bring their flocks to high-elevation pastures for extended summer periods (Nettier, Dobremez, Coussy, & Romagny, 2010). The greening trends we have documented here may further encourage such practices. This highlights that livestock farming systems cannot be solely envisaged as potential drivers of greening trends but that pastoral practices will also have to adapt to the changing productivity and spatial distribution of mountain pastures (Jager, Peratoner, Tappeiner, & Tasser, 2020).

Conclusion

In summary, the uplands of the European Alps have undergone widespread albeit non-uniform greening over the last two decades. High-elevation ecosystems have positively responded to ongoing summer warming with varying degrees of sensitivity. This conclusion is supported by the importance of predisposing factors such as the NDVImax anomaly, i.e. an abnormally low initial greenness, which explains a substantial portion of the spatial variability of greening. Sparsely vegetated ecosystems on north-facing slopes and experiencing

prolonged snow cover duration are the most highly responsive to ongoing warming, possibly because the positive effect of increased temperature is not dampened by limiting water supply and density-dependent plant competition. Our findings call for further studies examining why certain areas of the European Alps exhibit negative NDVImax anomalies and whether this determines specific ecological mechanisms underpinning observed greening trends.

Acknowledgements

This work received funding from the LIFE PASTORALP project (LIFE16 CCA/IT/000060). We acknowledge the E-OBS dataset from the EU-FP6 project UERRA (https://www.uerra.eu) and the Copernicus Climate Change Service, and the data providers in the ECA&D project (https://www.ecad.eu). Most of the computations presented in this paper were performed using the Froggy platform of the GRICAD infrastructure (*https://gricad.univ-grenoble-alpes.fr*), which is supported by the Rhône-Alpes region (GRANT CPER07_13 CIRA), the OSUG@2020 labex (reference ANR10 LABX56) and the Equip@Meso project (reference ANR-10-EQPX-29-01) of the Programme Investissements d'Avenir supervised by the Agence Nationale pour la Recherche. LECA is part of OSUG@2020 labex.

Supporting Information

Additional supporting information - three tables and 13 figures - may be found online in the Supporting Information section.

References

Anderson, K., Fawcett, D., Cugulliere, A., Benford, S., Jones, D., & Leng, R. L. (2020). Vegetation expansion in the subnival Hindu Kush Himalaya. *Global Change Biology, 26*(3), 1608-1625. doi:10.1111/gcb.14919

André, G., Lavergne, S., & Carcaillet, C. (2020). Unsuspected prevalent tree occurrences in high elevation sky-islands of the western Alps. *bioRxiv*, 2020.2007.2008.193300. doi:10.1101/2020.07.08.193300

Asam, S., Callegari, M., Matiu, M., Fiore, G., De Gregorio, L., Jacob, A., . . . Notarnicola, C. (2018). Relationship between Spatiotemporal Variations of Climate, Snow Cover and Plant Phenology over the Alps-An Earth Observation-Based Analysis. *Remote Sensing, 10*(11). doi:10.3390/rs10111757

Avanzi, F., Ercolani, G., Gabellani, S., Cremonese, E., Pogliotti, P., Filippa, G., . . . Cauduro, M. (2020). Learning about precipitation orographic enhancement from snow-course data improves water-balance modeling. *Hydrology and Earth System Sciences Discussions*, 1-37.

Beniston, M. (2006). Mountain weather and climate: A general overview and a focus on climatic change in the Alps. *Hydrobiologia, 562*, 3-16. doi:10.1007/s10750-005-1802-0

Berner, L. T., Massey, R., Jantz, P., Forbes, B. C., Macias-Fauria, M., Myers-Smith, I., . . . Goetz, S. J. (2020). Summer warming explains widespread but not uniform greening in the Arctic tundra biome. *Nature Communications, 11*(1). doi:10.1038/s41467-020-18479-5

Böhner, J., & Antonić, O. (2009). Land-surface parameters specific to topo-climatology. *Developments in soil science, 33*, 195-226.

597 Callaghan, T. V., Bergholm, F., Christensen, T. R., Jonasson, C., Kokfelt, U., & Johansson,
598 M. (2010). A new climate era in the sub-Arctic: Accelerating climate changes and
599 multiple impacts. *Geophysical Research Letters, 37*. doi:10.1029/2009gl042064
600 Cannone, N., Sgorbati, S., & Guglielmin, M. (2007). Unexpected impacts of climate change
601 on alpine vegetation. *Frontiers in Ecology and the Environment, 5*(7), 360-364.
602 doi:10.1890/1540-9295(2007)5[360:UIOCCO]2.0.CO;2
603 Carlson, B. Z., Corona, M. C., Dentant, C., Bonet, R., Thuiller, W., & Choler, P. (2017).
604 Observed long-term greening of alpine vegetation-a case study in the French Alps.
605 *Environmental Research Letters, 12*(11). doi:10.1088/1748-9326/aa84bd
606 Choler, P. (2015). Growth response of temperate mountain grasslands to inter-annual
607 variations in snow cover duration. *Biogeosciences, 12*(12), 3885-3897.
608 doi:10.5194/bg-12-3885-2015
609 Cornes, R. C., van der Schrier, G., van den Besselaar, E. J. M., & Jones, P. D. (2018). An
610 Ensemble Version of the E-OBS Temperature and Precipitation Data Sets. *Journal of*
611 *Geophysical Research-Atmospheres, 123*(17), 9391-9409. doi:10.1029/2017jd028200
612 Corona-Lozada, M. C., Morin, S., & Choler, P. (2019). Drought offsets the positive effect of
613 summer heat waves on the canopy greenness of mountain grasslands. *Agricultural and*
614 *Forest Meteorology, 276*. doi:10.1016/j.agrformet.2019.107617
615 Cortés, J., Mahecha, M. D., Reichstein, M., Myneni, R. B., Chen, C., & Brenning, A. (2021).
616 Where are Global Vegetation Greening and Browning Trends Significant?
617 *Geophysical Research Letters, 48*(6), e2020GL091496.
618 Dunn, A. H., & de Beurs, K. M. (2011). Land surface phenology of North American
619 mountain environments using moderate resolution imaging spectroradiometer data.
620 *Remote Sensing of Environment, 115*(5), 1220-1233. doi:10.1016/j.rse.2011.01.005

621 Durand, Y., Giraud, G., Laternser, M., Etchevers, P., Mérindol, L., & Lesaffre, B. (2009).
622 Reanalysis of 47 Years of Climate in the French Alps (1958–2005): Climatology and
623 Trends for Snow Cover. *Journal of Applied Meteorology and Climatology, 48*(12),
624 2487-2512. doi:10.1175/2009jamc1810.1
625 Duveiller, G., Hooker, J., & Cescatti, A. (2018). The mark of vegetation change on Earth's
626 surface energy balance. *Nature Communications, 9*. doi:10.1038/s41467-017-02810-8
627 EEA. (2009). Regional Climate Change Adaptation. The Alps Facing the Challenge of
628 Changing Water Resources. *European Environment Agency: Copenaghen, Denmark*.
629 Filippa, G., Cremonese, E., Galvagno, M., Isabellon, M., Bayle, A., Choler, P., . . .
630 Migliavacca, M. (2019). Climatic Drivers of Greening Trends in the Alps. *Remote*
631 *Sensing, 11*(21). doi:10.3390/rs11212527
632 Fontana, F., Rixen, C., Jonas, T., Aberegg, G., & Wunderle, S. (2008). Alpine grassland
633 phenology as seen in AVHRR, VEGETATION, and MODIS NDVI time series - a
634 comparison with in situ measurements. *Sensors, 8*(4), 2833-2853.
635 doi:10.3390/s8042833
636 Forzieri, G., Alkama, R., Miralles, D. G., & Cescatti, A. (2017). Satellites reveal contrasting
637 responses of regional climate to the widespread greening of Earth. *SCIENCE,*
638 *356*(6343), 1140-1144. doi:10.1126/science.aal1727
639 Francon, L., Corona, C., Till-Bottraud, I., Choler, P., Carlson, B. Z., Charrier, G., . . . Stoffel,
640 M. (2020). Assessing the effects of earlier snow melt-out on alpine shrub growth: The
641 sooner the better? *Ecological Indicators, 115*. doi:10.1016/j.ecolind.2020.106455
642 Frei, C., & Isotta, F. A. (2019). Ensemble Spatial Precipitation Analysis From Rain Gauge
643 Data: Methodology and Application in the European Alps. *Journal of Geophysical*
644 *Research-Atmospheres, 124*(11), 5757-5778. doi:10.1029/2018jd030004

Gehrig-Fasel, J., Guisan, A., & Zimmermann, N. E. (2007). Tree line shifts in the Swiss Alps: Climate change or land abandonment? *Journal of Vegetation Science, 18*(4), 571-582. doi:10.1111/j.1654-1103.2007.tb02571.x

Giaccone, E., Luoto, M., Vittoz, P., Guisan, A., Mariethoz, G., & Lambiel, C. (2019). Influence of microclimate and geomorphological factors on alpine vegetation in the Western Swiss Alps. *Earth Surface Processes and Landforms, 44*(15), 3093-3107. doi:10.1002/esp.4715

Gottfried, M., Pauli, H., Futschik, A., Akhalkatsi, M., Barancok, P., Alonso, J. L. B., . . . Grabherr, G. (2012). Continent-wide response of mountain vegetation to climate change. *Nature Climate Change, 2*(2), 111-115. doi:10.1038/nclimate1329

Greenwell, B. M. (2017). pdp: An R Package for Constructing Partial Dependence Plots. *The R Journal, 9*, 421-436.

Hansen, S. (1984). Estimation of Potential and Actual Evapotranspiration. *Nordic Hydrology, 15*(4-5), 205-212.

Hantel, M., & Hirtl-Wielke, L. M. (2007). Sensitivity of Alpine snow cover to European temperature. *International Journal of Climatology, 27*(10), 1265-1275. doi:10.1002/joc.1472

Harsch, M. A., Hulme, P. E., McGlone, M. S., & Duncan, R. P. (2009). Are treelines advancing? A global meta-analysis of treeline response to climate warming. *Ecology Letters, 12*(10), 1040-1049. doi:10.1111/j.1461-0248.2009.01355.x

Hinojosa, L., Napoleone, C., Moulery, M., & Lambin, E. F. (2016). The "mountain effect" in the abandonment of grasslands: Insights from the French Southern Alps. *Agriculture Ecosystems & Environment, 221*, 115-124. doi:10.1016/j.agee.2016.01.032

Hock, R., Rasul, G., Adler, C., Cáceres, B., Gruber, S., Hirabayashi, Y., . . . Steltzer, H. (2019). Chapter 2: High Mountain Areas.

http://report.ipcc.ch/srocc/pdf/SROCC_FinalDraft_Chapter2.pdf. In *In IPCC Special Report on Ocean and Cryosphere in a Changing Climate*.

Huete, A., Didan, K., Miura, T., Rodriguez, E. P., Gao, X., & Ferreira, L. G. (2002). Overview of the radiometric and biophysical performance of the MODIS vegetation indices. *Remote Sensing of Environment, 83*(1-2), 195-213. doi:10.1016/s0034-4257(02)00096-2

Jager, H., Peratoner, G., Tappeiner, U., & Tasser, E. (2020). Grassland biomass balance in the European Alps: current and future ecosystem service perspectives. *Ecosystem Services, 45*. doi:10.1016/j.ecoser.2020.101163

Jolly, W. M., Dobbertin, M., Zimmermann, N. E., & Reichstein, M. (2005). Divergent vegetation growth responses to the 2003 heat wave in the Swiss Alps. *Geophysical Research Letters, 32*(18), NIL_1-NIL_4.

Ju, J., & Masek, J. G. (2016). The vegetation greenness trend in Canada and US Alaska from 1984-2012 Landsat data. *Remote Sensing of Environment, 176*, 1-16. doi:10.1016/j.rse.2016.01.001

Keenan, T. F., & Riley, W. J. (2018). Greening of the land surface in the world's cold regions consistent with recent warming. *Nature Climate Change, 8*(9), 825-+. doi:10.1038/s41558-018-0258-y

Klein, G., Vitasse, Y., Rixen, C., Marty, C., & Rebetez, M. (2016). Shorter snow cover duration since 1970 in the Swiss Alps due to earlier snowmelt more than to later snow onset. *Climatic Change, 139*(3-4), 637-649. doi:10.1007/s10584-016-1806-y

Körner, C. (1999). *Alpine Plant Life*. Berlin: Springer Verlag.

Krakauer, N. Y., Lakhankar, T., & Anadon, J. D. (2017). Mapping and Attributing Normalized Difference Vegetation Index Trends for Nepal. *Remote Sensing, 9*(10). doi:10.3390/rs9100986

695 Kuhn, M. (2020). Caret: classification and regression training. R package version 6.0-86.
696 https://CRAN.R-project.org/package=caret.
697 Lamprecht, A., Semenchuk, P. R., Steinbauer, K., Winkler, M., & Pauli, H. (2018). Climate
698 change leads to accelerated transformation of high-elevation vegetation in the central
699 Alps. *New Phytologist, 220*(2), 447-459. doi:10.1111/nph.15290
700 Liaw, A., & Wiener, M. (2002). Classification and regression by randomForest. *R news, 2*(3),
701 18-22.
702 Liberati, L., Messerli, S., Matteodo, M., & Vittoz, P. (2019). Contrasting impacts of climate
703 change on the vegetation of windy ridges and snowbeds in the Swiss Alps. *Alpine*
704 *Botany, 129*(2), 95-105. doi:10.1007/s00035-019-00223-5
705 Mainetti, A., D'Amico, M., Probo, M., Quaglia, E., Ravetto Enri, S., Celi, L., & Lonati, M.
706 (2021). Successional Herbaceous Species Affect Soil Processes in a High-Elevation
707 Alpine Proglacial Chronosequence. *Frontiers in Environmental Science, 8*.
708 doi:10.3389/fenvs.2020.615499
709 Matiu, M., Crespi, A., Bertoldi, G., Carmagnola, C. M., Marty, C., Morin, S., . . . De
710 Gregorio, L. (2021). Observed snow depth trends in the European Alps: 1971 to 2019.
711 *The Cryosphere, 15*(3), 1343-1382. doi:10.5194/tc-15-1343-2021
712 Matteodo, M., Ammann, K., Verrecchia, E. P., & Vittoz, P. (2016). Snowbeds are more
713 affected than other subalpine-alpine plant communities by climate change in the Swiss
714 Alps. *Ecology and Evolution, 6*(19), 6969-6982. doi:10.1002/ece3.2354
715 McLeod, A. I. (2005). Kendall rank correlation and Mann-Kendall trend test. R package
716 version 2.2. https://CRAN.R-project.org/package=Kendall.
717 Miura, T., Huete, A. R., & Yoshioka, H. (2000). Evaluation of sensor calibration uncertainties
718 on vegetation indices for MODIS. *Ieee Transactions on Geoscience and Remote*
719 *Sensing, 38*(3), 1399-1409. doi:10.1109/36.843034

720 Motta, R., & Nola, P. (2001). Growth trends and dynamics in sub-alpine forest stands in the
721 Varaita Valley (Piedmont, Italy) and their relationships with human activities and
722 global change. *Journal of Vegetation Science, 12*(2), 219-230. doi:10.2307/3236606
723 Myers-Smith, I. H., Kerby, J. T., Phoenix, G. K., Bjerke, J. W., Epstein, H. E., Assmann, J. J.,
724 . . . Wipf, S. (2020). Complexity revealed in the greening of the Arctic. *Nature*
725 *Climate Change, 10*(2), 106-117. doi:10.1038/s41558-019-0688-1
726 Myneni, R. B., & Williams, D. L. (1994). On the Relationship between FAPAR and NDVI.
727 *Remote Sensing of Environment, 49*(3), 200-211. doi:10.1016/0034-4257(94)90016-7
728 Napoli, A., Crespi, A., Ragone, F., Maugeri, M., & Pasquero, C. (2019). Variability of
729 orographic enhancement of precipitation in the Alpine region. *Scientific Reports, 9*.
730 doi:10.1038/s41598-019-49974-5
731 Nettier, B., Dobremez, L., Coussy, J.-L., & Romagny, T. (2010). Attitudes of livestock
732 farmers and sensitivity of livestock farming systems to drought conditions in the
733 French Alps. *Revue De Geographie Alpine-Journal of Alpine Research, 98*(1-4), 383-
734 400. doi:10.4000/rga.1307
735 Palazzi, E., Mortarini, L., Terzago, S., & von Hardenberg, J. (2019). Elevation-dependent
736 warming in global climate model simulations at high spatial resolution. *Climate*
737 *Dynamics, 52*(5-6), 2685-2702. doi:10.1007/s00382-018-4287-z
738 Pepin, N., Bradley, R. S., Diaz, H. F., Baraer, M., Caceres, E. B., Forsythe, N., . . . Mt Res
739 Initiative, E. D. W. W. G. (2015). Elevation-dependent warming in mountain regions
740 of the world. *Nature Climate Change, 5*(5), 424-430. doi:10.1038/nclimate2563
741 Randin, C. F., Ashcroft, M. B., Bolliger, J., Cavender-Bares, J., Coops, N. C., Dullinger, S., . .
742 . Payne, D. (2020). Monitoring biodiversity in the Anthropocene using remote sensing
743 in species distribution models. *Remote Sensing of Environment, 239*.
744 doi:10.1016/j.rse.2019.111626

745 Rixen, C., Wipf, S., Frei, E., & Stoeckli, V. (2014). Faster, higher, more? Past, present and
746 future dynamics of alpine and arctic flora under climate change. *Alpine Botany,*
747 *124*(2), 77-79. doi:10.1007/s00035-014-0141-z
748 Rogora, M., Frate, L., Carranza, M. L., Freppaz, M., Stanisci, A., Bertani, I., . . . Matteucci,
749 G. (2018). Assessment of climate change effects on mountain ecosystems through a
750 cross-site analysis in the Alps and Apennines. *Science of the Total Environment, 624*,
751 1429-1442. doi:10.1016/j.scitotenv.2017.12.155
752 Ropars, P., & Boudreau, S. (2012). Shrub expansion at the forest-tundra ecotone: spatial
753 heterogeneity linked to local topography. *Environmental Research Letters, 7*(1).
754 doi:10.1088/1748-9326/7/1/015501
755 Ropars, P., Levesque, E., & Boudreau, S. (2015). Shrub densification heterogeneity in
756 subarctic regions: the relative influence of historical and topographic variables.
757 *Ecoscience, 22*(2-4), 83-95. doi:10.1080/11956860.2015.1107262
758 Savitzky, A., & Golay, M. J. E. (1964). Smoothing and Differentiation of Data by Simplified
759 Least Squares Procedures. *Analytical Chemistry, 36*, 1627-1639.
760 Schoener, W., Koch, R., Matulla, C., Marty, C., & Tilg, A.-M. (2019). Spatiotemporal
761 patterns of snow depth within the Swiss-Austrian Alps for the past half century (1961
762 to 2012) and linkages to climate change. *International Journal of Climatology, 39*(3),
763 1589-1603. doi:10.1002/joc.5902
764 signal developpers. (2013). signal: Signal processing. http://r-forge.r-
765 project.org/projects/signal/.
766 Steinbauer, M. J., Grytnes, J.-A., Jurasinski, G., Kulonen, A., Lenoir, J., Pauli, H., . . . Wipf,
767 S. (2018). Accelerated increase in plant species richness on mountain summits is
768 linked to warming. *Nature, 556*(7700), 231-+. doi:10.1038/s41586-018-0005-6

769 Sturm, M., Schimel, J., Michaelson, G., Welker, J. M., Oberbauer, S. F., Liston, G. E., . . .
770 Romanovsky, V. E. (2005). Winter biological processes could help convert arctic
771 tundra to shrubland. *Bioscience, 55*(1), 17-26. doi:10.1641/0006-
772 3568(2005)055[0017:wbpchc]2.0.co;2
773 Suding, K. N., Farrer, E. C., King, A. J., Kueppers, L., & Spasojevic, M. J. (2015). Vegetation
774 change at high elevation: scale dependence and interactive effects on Niwot Ridge.
775 *Plant Ecology & Diversity, 8*(5-6), 713-725. doi:10.1080/17550874.2015.1010189
776 Tape, K. D., Hallinger, M., Welker, J. M., & Ruess, R. W. (2012). Landscape Heterogeneity
777 of Shrub Expansion in Arctic Alaska. *Ecosystems, 15*(5), 711-724.
778 doi:10.1007/s10021-012-9540-4
779 Tape, K. D., Sturm, M., & Racine, C. (2006). The evidence for shrub expansion in Northern
780 Alaska and the Pan-Arctic. *Global Change Biology, 12*(4), 686-702.
781 doi:10.1111/j.1365-2486.2006.01128.x
782 Tappeiner, U., Borsdorf, A., & Tasser, E. (2008). *Mapping the Alps: Society - Economy -*
783 *Environment*. Heidelberg: Spektrum Akademischer Verlag.
784 Tucker, C. J. (1979). Red and photographic infrared linear combinations for monitoring
785 vegetation. *Remote Sensing of Environment, 8*(2), 127-150. doi:10.1016/0034-
786 4257(79)90013-0
787 Venables, W., & Ripley, B. (2002). *Modern applied statistics (Fourth S., editor) New York*:
788 Springer.
789 Verbesselt, J., Hyndman, R., Newnham, G., & Culvenor, D. (2010). Detecting trend and
790 seasonal changes in satellite image time series. *Remote Sensing of Environment,*
791 *114*(1), 106-115. doi:10.1016/j.rse.2009.08.014
792 Vermote, E., & Vermeulen, A. (1999). Atmospheric correction algorithm: spectral
793 reflectances (MOD09). *ATBD version, 4*, 1-107.

794 Vernay, M., Lafaysse, M., Hagenmuller , P., Nheili , R., Verfaillie , D., & Morin , S. (2019).
795 The S2M meteorological and snow cover reanalysis in the French mountainous areas
796 (1958 - present). Dataset. https://doi.org/10.25326/37.
797 Vionnet, V., Six, D., Auger, L., Dumont, M., Lafaysse, M., Queno, L., . . . Vincent, C. (2019).
798 Sub-kilometer Precipitation Datasets for Snowpack and Glacier Modeling in Alpine
799 Terrain. *Frontiers in Earth Science, 7*. doi:10.3389/feart.2019.00182
800 Viovy, N., Arino, O., & Belward, A. S. (1992). The Best Index Slope Extraction (BISE) - a
801 method for reducing noise in NDVI time-series. *International Journal of Remote*
802 *Sensing, 13*(8), 1585-1590. doi:10.1080/01431169208904212
803 Vittoz, P., Bodin, J., Ungricht, S., Burga, C., & Walther, G. R. (2008). One century of
804 vegetation change on Isla Persa, a nunatak in the Bernina massif in the Swiss Alps.
805 *Journal of Vegetation Science, 19*(5), 671-U628. doi:10.3170/2008-8-18434
806 Vittoz, P., Rulence, B., Largey, T., & Frelechoux, F. (2008). Effects of climate and land-use
807 change on the establishment and growth of cembran pine (Pinus cembra L.) over the
808 altitudinal treeline ecotone in the Central Swiss Alps. *Arctic Antarctic and Alpine*
809 *Research, 40*(1), 225-232. doi:10.1657/1523-0430(06-010)[vittoz]2.0.co;2
810 Vorkauf, M., Marty, C., Kahmen, A., & Hiltbrunner, E. (2021). Past and future snowmelt
811 trends in the Swiss Alps: the role of temperature and snowpack. *Climatic Change,*
812 *165*(3), 1-19.
813 Xie, J., Jonas, T., Rixen, C., de Jong, R., Garonna, I., Notarnicola, C., . . . Kneubuehler, M.
814 (2020). Land surface phenology and greenness in Alpine grasslands driven by
815 seasonal snow and meteorological factors. *Science of the Total Environment, 725*.
816 doi:10.1016/j.scitotenv.2020.138380
817 Zhang, G., Zhang, Y., Dong, J., & Xiao, X. (2013). Green-up dates in the Tibetan Plateau
818 have continuously advanced from 1982 to 2011. *Proceedings of the National Academy*

819 *of Sciences of the United States of America, 110*(11), 4309-4314.
820 doi:10.1073/pnas.1210423110
821 Zhao, M., & Running, S. W. (2010). Drought-Induced Reduction in Global Terrestrial Net
822 Primary Production from 2000 Through 2009. *SCIENCE, 329*(5994), 940-943.
823 doi:10.1126/science.1192666
824 Zhu, Z., Piao, S., Myneni, R. B., Huang, M., Zeng, Z., Canadell, J. G., . . . Zeng, N. (2016).
825 Greening of the Earth and its drivers. *Nature Climate Change, 6*(8), 791-+.
826 doi:10.1038/nclimate3004
827

Figure legends

Figure 1 Sign and magnitude of greenness trends in above-treeline ecosystems of European Alps. a Frequency distribution of linear trends of NDVImax over the period 2000-2020. Slopes were estimated using the Theil–Sen median slope analysis. Levels of significance were assessed by a non-parametric, rank based, Mann–Kendall (MK) monotonic test. Positive [negative] values correspond to greening [browning] trends. The analysis was performed on 284 546 pixels at 250 m resolution. **b** Greenness trends by land cover class. The European-scale product Corine Land Cover (CLC) was utilized. Note that the CLC class "bare rocks" was renamed "very sparsely vegetated" as the average NDVImax of selected pixels was above 0.1. Note the different scale for positive and negative trends.

Figure 2 Spatial distribution of greenness trends. To ease reading, we applied a 5x5 pixels moving window to the original 250 m resolution map. The color scale represents the percentage of pixels showing significant greening ($P < 0.05$) over the period 2000-2020. The bold line delineates the European Alps whose location is shown in the upper left insert. The lower right insert allows visualizing regional hotspots of greening by aggregating the 250 m resolution map at 2.5 km and by coloring pixels for which more than 80% of the 250 m pixels exhibited fast greening ($P < 0.005$).

Figure 3 Variation of greenness trends along gradients of elevation and diurnal anisotropic heating (DAH). a Heatmap of the mean value of NDVImax slopes per class of elevation and DAH. Only combinations representing more than 5% of the total number of pixels are shown. **b** Elevational distribution of three ranges of NDVImax along the gradient of DAH. Lines indicate the second decile, the median and the eighth decile of the distribution. Average NDVImax values are shown for three 10-year sliding windows.

Figure 4 Anomalies of NDVImax. a An example of the variation of NDVImax along elevation for DAH values in the interval]-0.25;-0.2]. NDVImax values are averages for the period 2000-2020. Black lines indicate the first, the fifth (median) and the ninth deciles of the distribution. The color palette from brown to green allows visualizing the NDVImax anomaly, i.e. the difference between NDVImax and the median value of the corresponding elevation x DAH combination. **b** Spatial distribution of the NDVImax anomaly in the European Alps. To ease reading, we applied a 5x5 moving window to the original 250 m resolution map.

Figure 5 Predictors of greenness trends. We classified pixels into three categories - no greening, moderate greening ($0.005<P<0.05$) and fast greening ($P<0.005$) - and implemented a random forest model to assess the importance of predictors. **a** Usefulness of the predictor for classification measured by the mean accuracy decrease in classification following permutation of variables. **b** Contribution of a predictor to the purity of nodes measured by the decrease in the Gini coefficient. **c** Partial dependency analyses showing the classification probability as a function of the set of values taken by the predictors. We created 1000 perturbed datasets of MODIS reflectances for the 284,346 pixels and then randomly selected 30,000 pixels in each dataset. These subsets of pixels were split into training (66%) and validation (33%) to implement the random forest model. Envelopes show the first and ninth deciles of the distribution.

Figure 6 Relationships between land cover, NDVImax anomalies and greenness trends. We randomly selected 100 pixels (500 m resolution) in three data subsets exhibiting negative, null and positive NDVImax anomalies (see Figure S7) and visually photo-interpreted land cover using very high resolution Google Earth imagery. Cover of

877 screes/outcrops (a) and grasslands (c) per class of NDVImax anomaly. NDVImax slopes
878 (mean +/- se) for each class of NDVImax anomaly distinguishing the cover of screes/outcrops
879 (c) and grasslands (d). Results of a post-hoc Tukey tests are denoted with letters. Different
880 lower case letters indicate a significant ($P<0.05$) difference within NDVImax anomaly class.
881 Different upper case letters indicate a significant ($P<0.05$) difference between NDVImax
882 anomaly class.

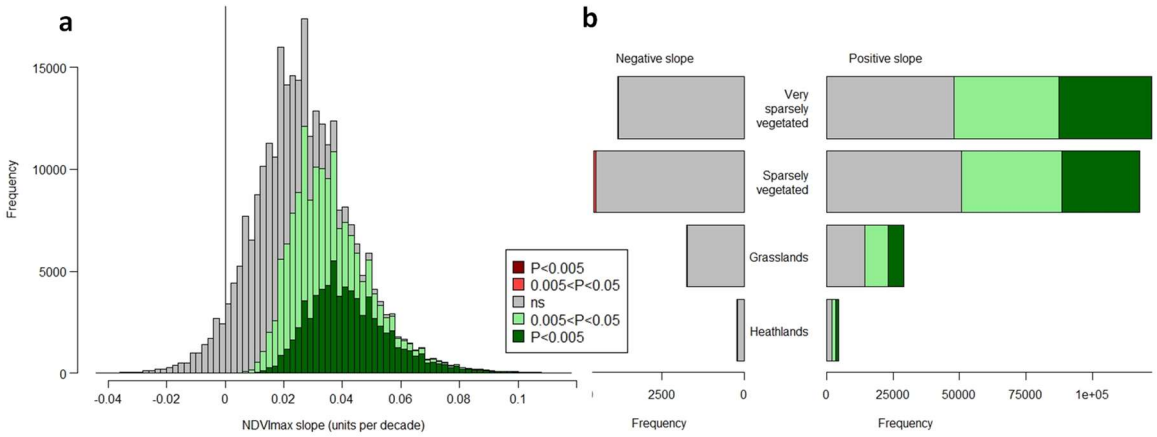

883

884 **Figure 1**

885

886

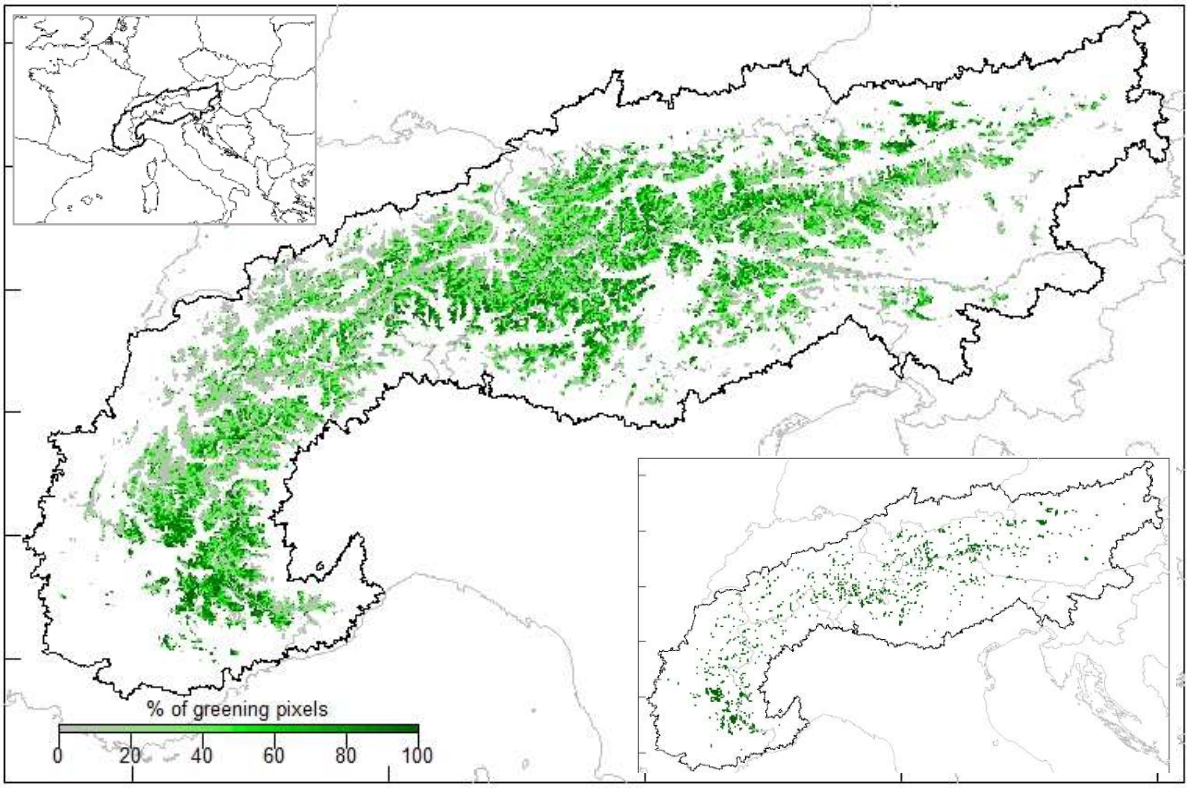

887

888 **Figure 2**

889

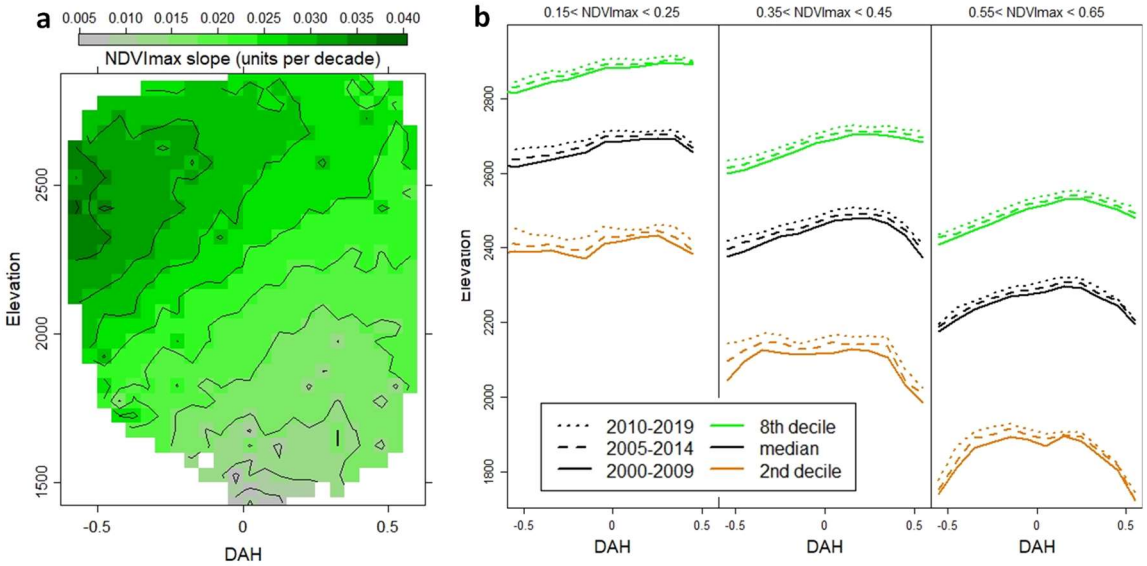
a
0.005 0.010 0.015 0.020 0.025 0.030 0.035 0.040
NDVImax slope (units per decade)
Elevation
1500
2000
2500
-0.5
0
0.5
DAH
b
0.15< NDVImax < 0.25
0.35< NDVImax < 0.45
0.55< NDVImax < 0.65
Elevation
1800
2000
2200
2400
2600
2800
2010-2019
2005-2014
2000-2009
8th decile
median
2nd decile
DAH

Figure 3

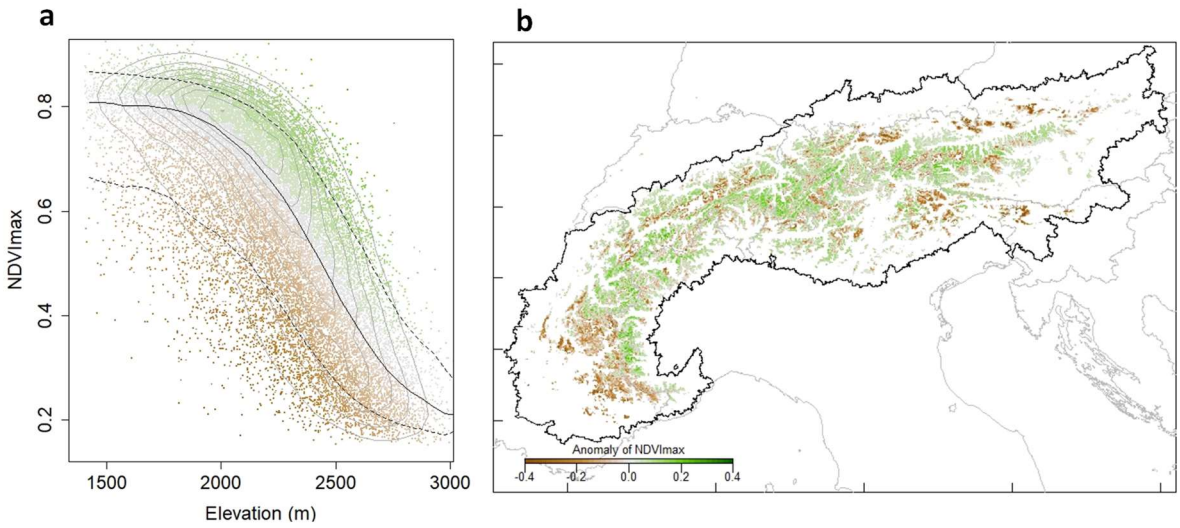
a
b
NDVImax
0.2
0.4
0.6
0.8
1500
2000
2500
3000
Elevation (m)
Anomaly of NDVImax
-0.4
-0.2
0.0
0.2
0.4

Figure 4

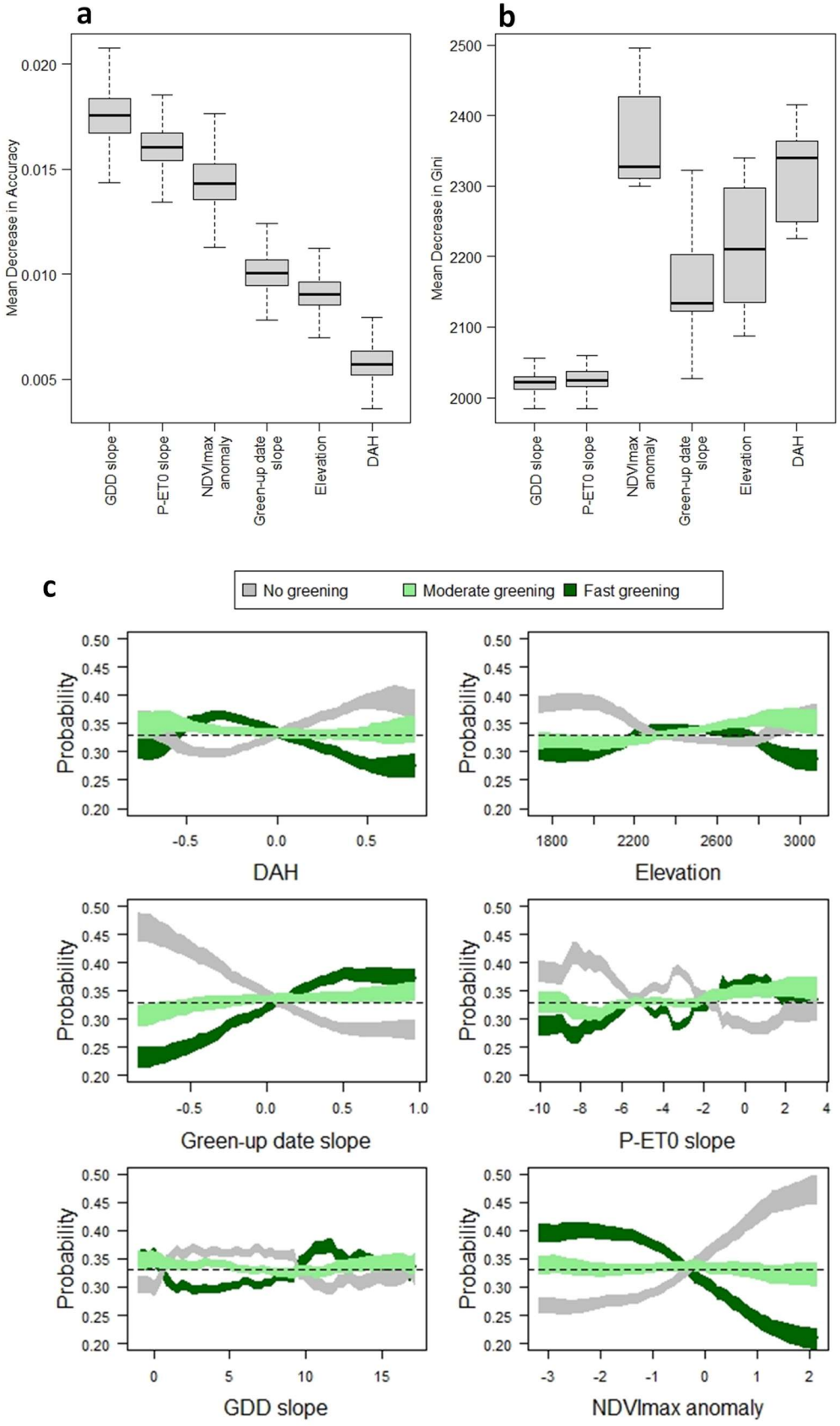
a
Mean Decrease in Accuracy
0.020
0.015
0.010
0.005
GDD slope
P-ET0 slope
NDVImax anomaly
Green-up date slope
Elevation
DAH
b
Mean Decrease in Gini
2500
2400
2300
2200
2100
2000
GDD slope
P-ET0 slope
NDVImax anomaly
Green-up date slope
Elevation
DAH
c
No greening
Moderate greening
Fast greening
Probability
DAH
Elevation
Green-up date slope
P-ET0 slope
GDD slope
NDVImax anomaly

Figure 5

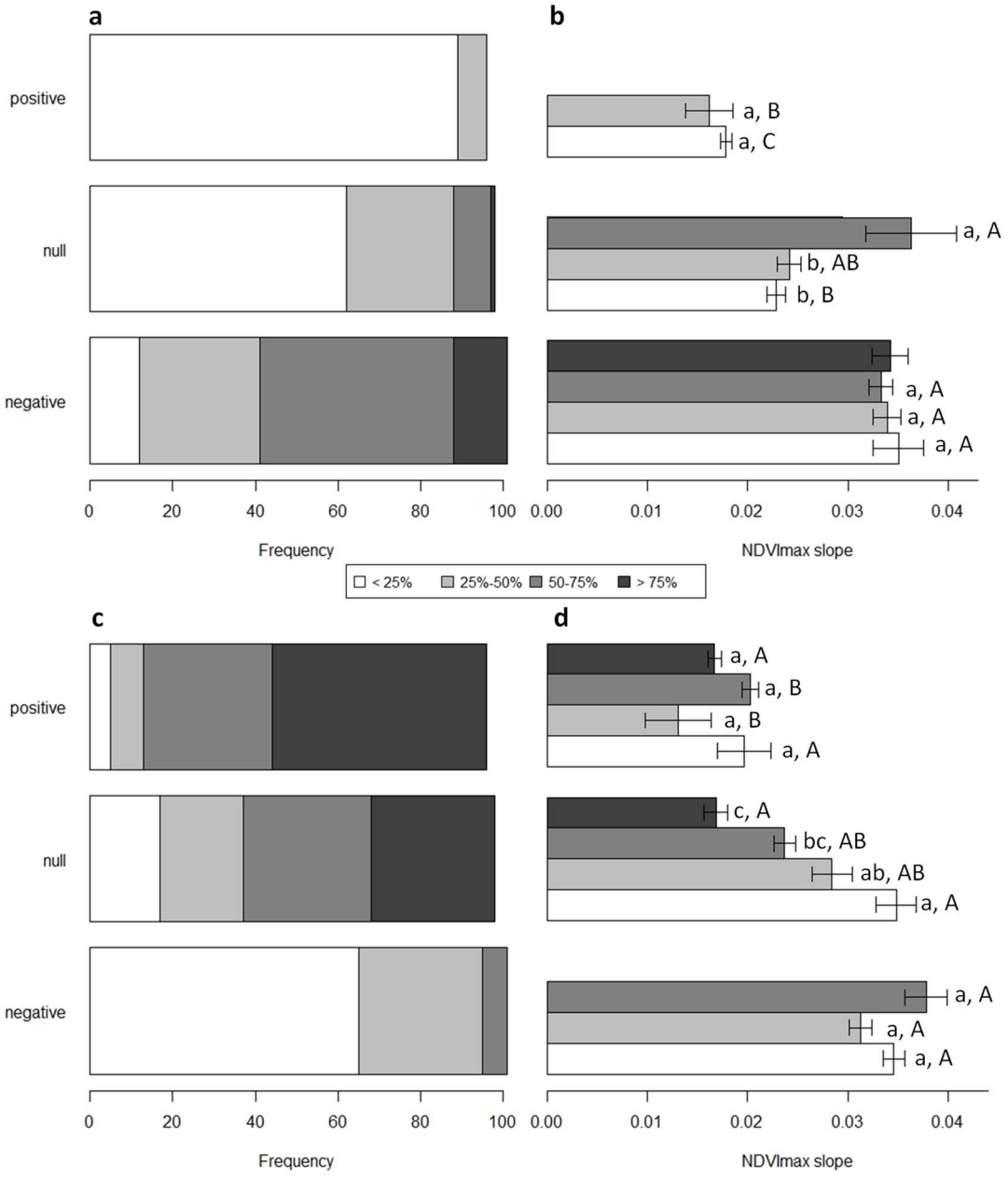
a
b
positive
null
negative
a, B
a, C
a, A
b, AB
b, B
a, A
a, A
a, A
0
20
40
60
80
100
0.00
0.01
0.02
0.03
0.04
Frequency
NDVImax slope
< 25%
25%-50%
50-75%
> 75%
c
d
positive
null
negative
a, A
a, B
a, B
a, A
c, A
bc, AB
ab, AB
a, A
a, A
a, A
a, A
0
20
40
60
80
100
0.00
0.01
0.02
0.03
0.04
Frequency
NDVImax slope

Figure 6